Supplementary Figure 1

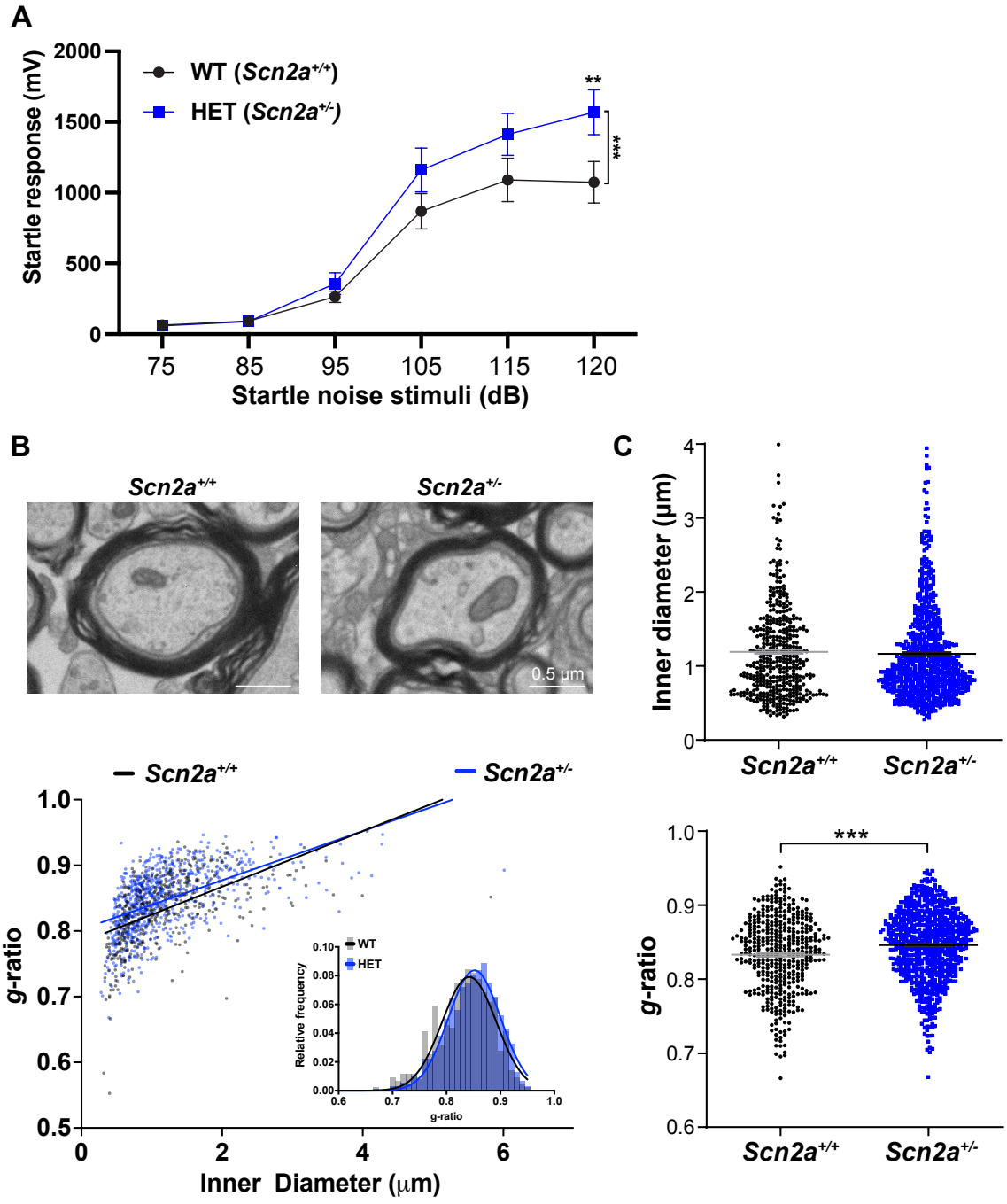

Supplementary figure 1. Auditory hypersensitivity and myelin abnormality were observed in *Scn2a*$^{+/-}$ mice. A. In an acoustic startle reflex test, *Scn2a*$^{+/-}$ mice (heterogynous mice; HET, n=13) showed higher startle response to sound stimuli (from 75 dB to 120 dB) compared to wild type mice (WT, *Scn2a* $^{+/+}$, n=14, p=0.0002, two-way ANOVA test with multiple comparison). **B.** (Top) Representative transmission electron microscopy (TEM) images of an axon in the MNTB from *Scn2a*$^{+/+}$ and *Scn2a*$^{+/-}$ mice. (Bottom) Scatter plot of *g*-ratio values, plotted as a function of corresponding axon inner diameter of individual axons, showed an up-shifted linear regression in *Scn2a*$^{+/-}$ mice (Blue) compared to *Scn2a* $^{+/+}$ (Black). The *g*-ratio is an indicator of myelin thickness measured by the inner radius (r) divided by the outer radius (R) of axon in the corresponding axon bundles. Inset, the histogram of the distribution of *g*-ratio. **C.** Summary of inner diameter (Top) and *g*-ratio (Bottom) of individual axons. The *g*-ratio was significantly higher in *Scn2a*$^{+/-}$ mice compared to *Scn2a*$^{+/+}$ without a significant difference in axon diameter (*g*-ratio, 0.83 ± 0.003, n = 439 axons in 5 *Scn2a*$^{+/+}$ mice vs 0.85 ± 0.002, n = 768 axons in 4 *Scn2a*$^{+/-}$ mice, $p < 0.0001$, Mann-Whitney *U*-test), indicating myelin thickness is reduced in *Scn2a*$^{+/-}$ mice.

Supplementary figure 3

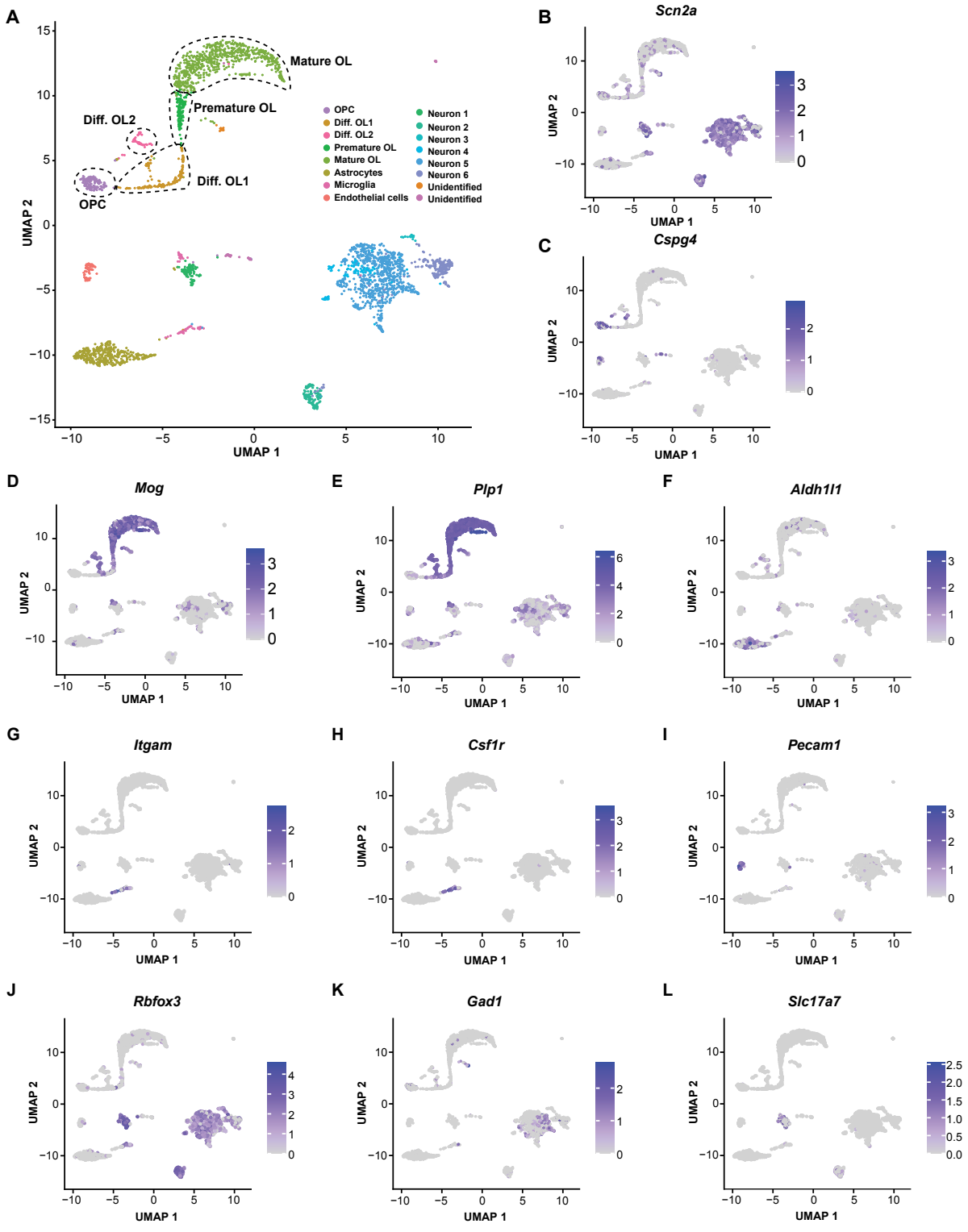

Supplementary figure 2. Cell populations and expression patterns of cell specific markers in snRNA-seq. A. Total 16 genetic clusters identified by Shared Nearest Neighbor (SNN) method were plotted using UMAP. **B-L.** Each cell type of the clusters was identified with expression patterns of cell specific markers. **(B)** Expression of *Scn2a*, which was strongly expressed in neurons. Notably, it was also detected across the OL lineage, supporting *Scn2a* expression and function in the OL lineage. The expression of cell specific markers; *Cspg4* for OPC **(C)**, Mog and *Plp1* for mature OL **(D, E)**, *Aldh1l1* for astrocyte **(F)**, *Itgam* and *Csf1r* for microglia **(G, H)** , *Pecam1* for epithelia cell **(I)**, *Rbfox3* for neuron **(J)**, *Gad1* for inhibitory neuron **(K)**, and *Slc17a7* for glutamatergic neuron **(L)**. Scaled expression level was color coded on the side of each plot.

Supplementary figure 3

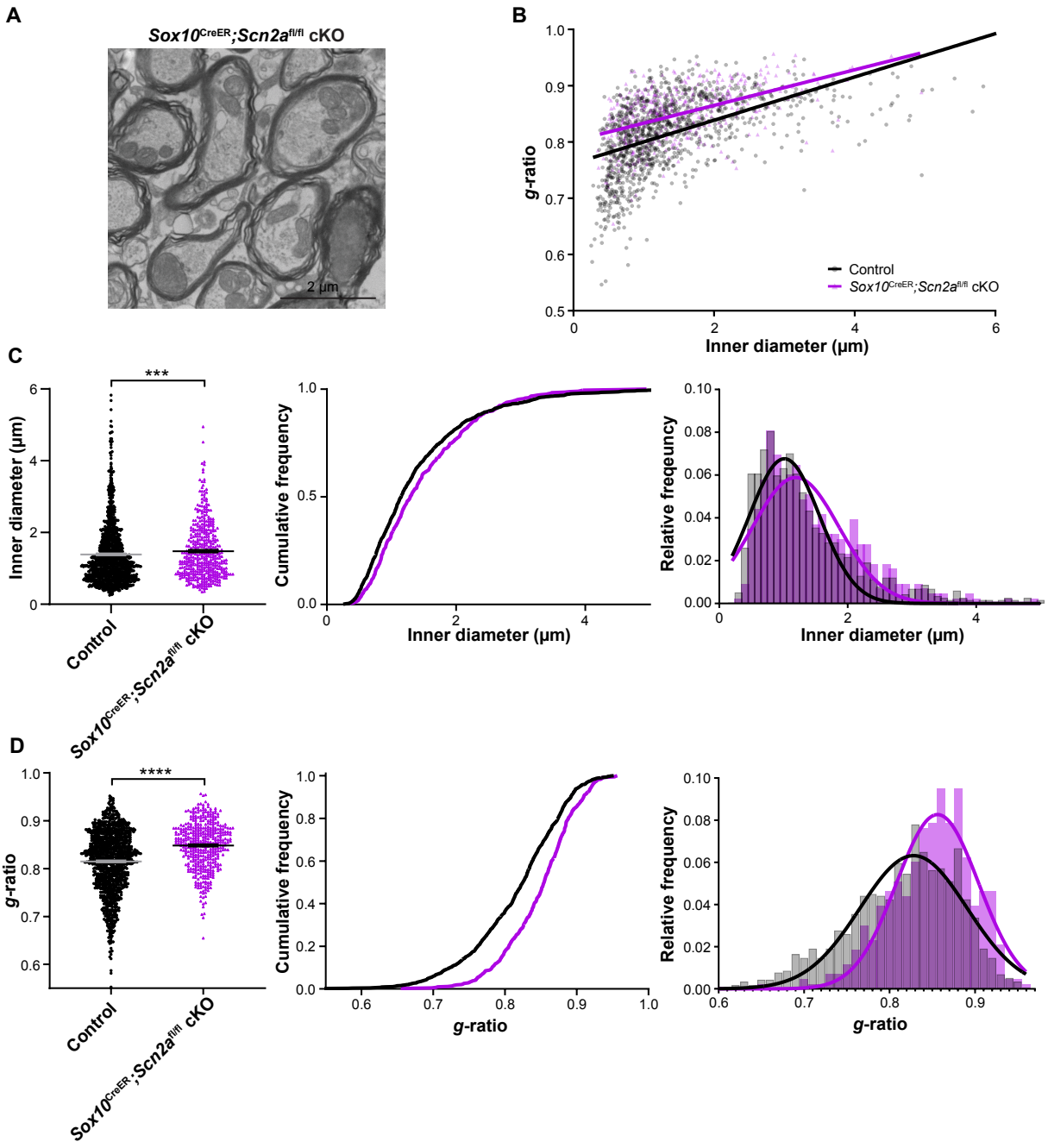

Supplementary figure 3. Axon caliber and myelin thickness deficits from *Scn2a* cKO mice. **A.** Representative TEM image of axons in the MNTB region from a different OL-specific cKO mouse line (*Sox10*^{CreER}; *Scn2a*$^{fl/fl}$, at P25) with an inducible *Sox10* Cre (*Sox10*^{CreER}) targeting all OL lineage cells. **B.** Scatter plot of *g*-ratio values plotted as a function of corresponding axon inner diameter of individual axons in the MNTB region. Datapoints from individual axons and best fit lines are shown in black for control and purple for *Scn2a* cKO mice (*Sox10*^{CreER}; *Scn2a*$^{fl/fl}$). **C.** Summary of inner diameter of individual axons (left), their respective cumulative frequency (middle), and the histogram distribution of inner diameter (right). The axon diameter was significantly increased in *Scn2a* cKO mice compared to control (*Scn2a*$^{fl/fl}$) without a significant difference in axon diameter (1.39 ± 0.03 μm, n = 1154 axons in 10 control mice vs 1.48 ± 0.04 μm, n = 432 axons in 3 *Scn2a* cKO mice, $p < 0.001$, Mann-Whitney *U*-test). The right shift of the cumulative frequency curve indicates an increase in axon caliber size in *Scn2a* cKO compared to control. **D.** Summary of *g*-ratio of individual axons (left), their respective cumulative frequency (middle), and the histogram of distribution of *g*-ratio (right). The *g*-ratio was significantly higher in *Scn2a* cKO mice (0.82 ± 0.002, n = 1154 axons in 10 control vs 0.85 ± 0.002, n = 432axons in 3 *Scn2a* cKO mice, $p < 0.0001$, Mann-Whitney *U*-test). In addition, there was also a right shift in the cumulative frequency distribution of *g*-ratio in *Scn2a* cKO, indicating *g*-ratio was larger in *Scn2a* cKO across examined axons Note that *Scn2a* cKO mice targeting all OL lineage cells also exhibit a higher *g*-ratio and larger inner diameter of axons in the auditory brainstem, indicating alterations in myelination and axonal integrity. Values are shown as mean ± s.e.m., *** $p < 0.001$, **** $p < 0.0001$.

Supplementary figure 4

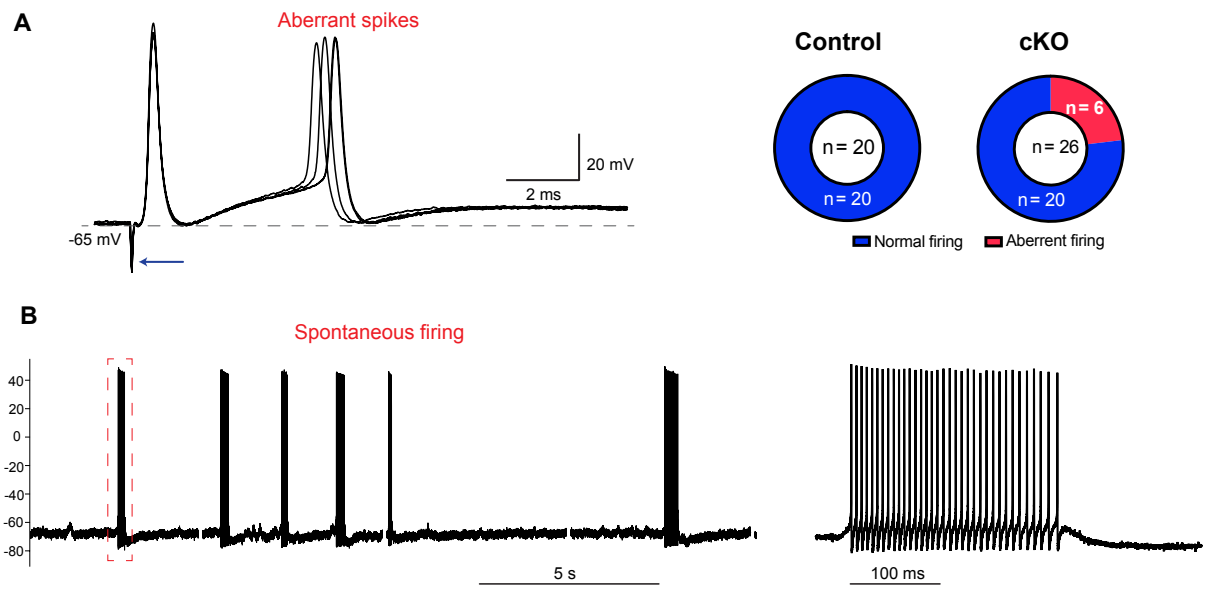

Supplementary figure 4. Aberrant spikes and spontaneous firing are present in some calyx terminals from *Scn2a* cKO mice. A. Left, representative trace of aberrant spikes at the calyx terminal responding to a single stimulus (arrow). In *Scn2a* cKO mice (*Pdgfra*^{CreERT}; *Scn2a*$^{fl/fl}$), APs were evoked by afferent fiber stimulus with high temporal fidelity but followed by aberrant spikes with "jitter". Right, ~25% of calyces (6/26 cells in *Scn2a* cKO) exhibited this abnormal spiking. However, all recordings from control did not show any aberrant spikes or spontaneous firing (0/20 cells in control). Arrow indicates the stimulus artifact caused by afferent fiber stimulation. **B.** Left, representative trace for spontaneous firing. The calyces (~25%) displayed spontaneous firing around -65 mV with a bursting rate of 200 Hz (without afferent fiber stimulation). Right, expanded view of the burst spiking in box.

Supplementary figure 5

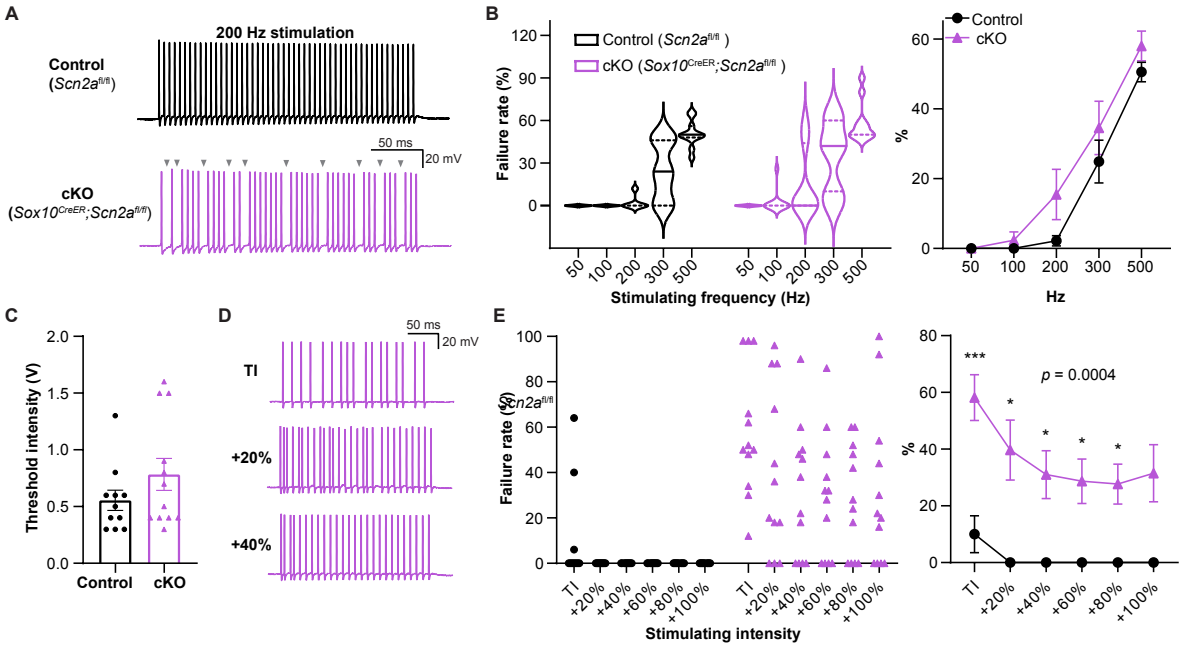

Supplementary figure 5. Conduction failures at the calyx terminals from *Scn2a* cKO mice. **A.** Representative traces of presynaptic APs from control (black) and *Scn2a* cKO mice (*Sox10*^{CreER}; *Scn2a*$^{fl/fl}$, purple) stimulated at 200 Hz. Grey arrowheads indicate absent APs. **B.** Left, violin plots showing AP failure rate from control and *Scn2a* cKO mice stimulated at varied frequencies. Solid and dashed lines represent median and first and third quartile, respectively. Right, average AP failure rate at varied stimulating frequencies. **C.** Average threshold intensity (TI) to initiate a single AP from control and *Scn2a* cKO mice. Individual datapoints are displayed as circles and triangles. **D.** Representative traces of 200 Hz AP train from *Scn2a* cKO mice stimulated with TI, 20% increment from TI, and 40% increment from TI. **E.** Left, 200 Hz AP failure rate of individual cells from incremental stimulating intensities. Right, average 200 Hz AP failure rate from incremental stimulating intensities (mean ± s.e.m.). * $p < 0.05$, *** $p < 0.001$.

Supplementary figure 6

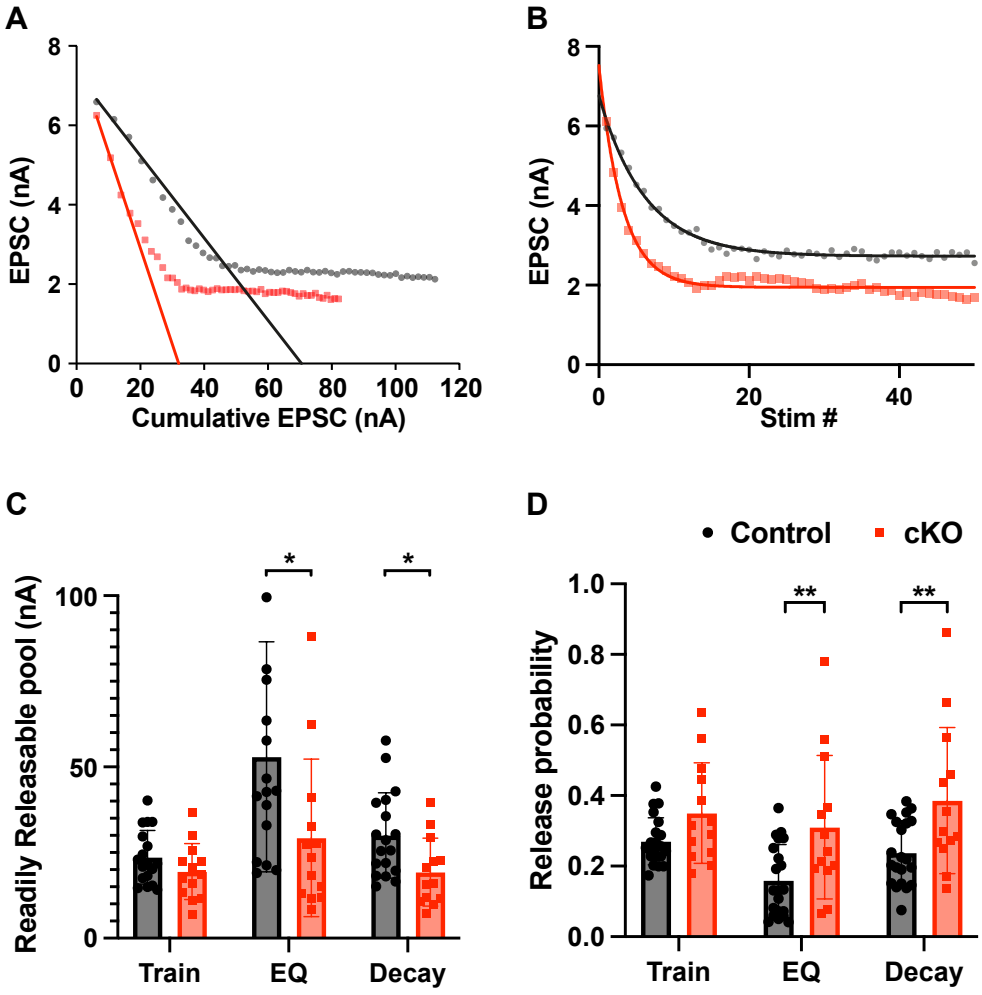

Supplementary figure 6. Different analysis methods showed similar changes in readily releasable pool (RRP) and release probability (Pr) in *Scn2a* cKO mice. A-B. Along with train method, the Elmqvist and Quastel (EQ) and the decay methods were also used to analyze the presynaptic properties. In the EQ method, the RRP size is estimated by fitting a line to the linear portion of these data (corresponding to the second through the fourth EPSC) and extrapolating to the x axis, we measured the total equivalent EPSC at the beginning of the train, which directly indicates the available pool of vesicles for release (**A**). In the decay method, the RRP size is estimated by fitting an exponential decay (B). **C-D.** Comparison of the RRP size and Pr using different methods; Using the EQ method, plotting the eEPSC amplitudes during a train versus their cumulative amplitudes at the end of a train, which were 52.94 ± 8.40 nA (n = 16) in control and 29.32 ± 6.38 nA (n = 13) in cKO mice (p=0.0404, unpaired t-test, **C**). Pr is determined as the slop of the linear fit (0.16 ± 0.022 in control and 0.31 ± 0.056 in cKO mice, p=0.0071, unpaired t-test, **D**). Using the decay method, the RRP was 30.0 ± 2.94 nA (n = 18) in control and 19.3 ± 2.76 nA (n = 13) in cKO mice (p=0.0157, unpaired t-test, **C**), and Pr was 0.238 ± 0.020 (n = 21) in control and 0.386 ± 0.057 (n = 13) in cKO mice (p=0.0071, unpaired t-test, D). * $p < 0.05$, ** $p < 0.01$, **** $p < 0.0001$.